ACS OMEGA

Open Access

http://pubs.acs.org/journal/acsodf

Article

Understanding Matrix Stiffness in Vinyl Polymer Hydrogels: Implications in Bone Tissue Engineering

Gyanendra Prasad Panda, Debyashreeta Barik, and Mamoni Dash*

Cite This: *ACS Omega* 2024, 9, 17891−17902

Read Online

ACCESS | Metrics & More | Article Recommendations | Supporting Information

ABSTRACT: Matrix elasticity helps to direct bone cell differentiation, impact healing processes, and modify extracellular matrix deposition, all of which are required for tissue growth and maintenance. In this work, we evaluated the role of inorganic nanocrystals or mineral inducers such as nanohydroxyapatite, alkaline phosphatase, and nanoclay also known as montmorillonite deposited on vinyl-based hydrogels in generating matrices with different stiffness and their role in cell differentiation. Poly-2-(dimethylamino)ethyl methacrylate (PD) and poly-2-hydroxypropylmethacrylamide (PH) are the two types of vinyl polymers chosen for preparing hydrogels via thermal cross-linking. The hydrogels exhibited porosity, which decreased with an increase in stiffness. Each of the compositions is non-cytotoxic and maintains the viability of pre-osteoblasts (MC3T3-E1) and human bone marrow mesenchymal stem cells (hBMSCs). The PD hydrogels in the presence of ALP showed the highest mineralization ability confirmed through the alizarin assay and a better structural environment for their use as scaffolds for tissue engineering. The study reveals that understanding such interactions can generate hydrogels that can serve as efficient 3D models to study biomineralization.

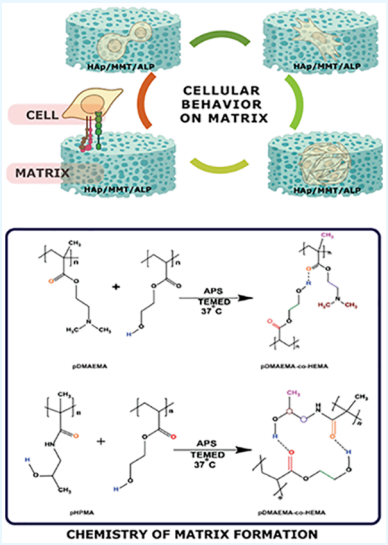

CHEMISTRY OF MATRIX FORMATION

1. INTRODUCTION

Hydrogels are water-containing 3D networks of polymers with both soft and wet properties due to the involvement of polymer chains and water in the 3D network.[1−7] Vinyl compounds such as N-isopropylacrylamide (NIPAAm), 2-(dimethylamino)ethyl methacrylate (DMAEMA),[7] and 2-hydroxypropyl methacrylate (HPMA)[8] are useful precursors for hydrogels due to their structural diversity. This class of polymers has been the subject of extensive research over the past few decades. They are appealing materials due to their ease of synthesis and wide range of topologies, compositions, and functions.[9] With their highly hydrated 3D polymer networks, vinylic hydrogels are appealing biomaterials for tissue regeneration, particularly bone regeneration.[10] Furthermore, hydrogels with mineralization precursors such as calcium phosphate (CaP)/silica layer are considered beneficial for bone regeneration applications.[11] Numerous biomimetic strategies have been used so far for developing pre-mineralized hydrogels.[12,13] Hydrogels' structure and hydrated nature allow for simple entry of ions such as calcium, phosphate, and silicates, whose delivery can be customized by varying their concentration in the local environment using appropriate mineralization solutions or sophisticated ion diffusion control devices. The process of hydrogel preparation using these polymers allows simple entrapment of mineralization-promoting elements during hydrogel polymer network creation.[14,15] It has been observed that substrates with different stiffness can have varied mineralization effects, as well as different degrees of cell proliferation and differentiation, with moderately stiff substrates promoting cell proliferation and differentiation.[16] However, the correlation between various stiffness generated by mineralized surfaces and their effect on cell differentiation is not well documented. In this study, the hydrogel elasticities are varied using mineral inducers or mineral precursors, namely, nHAp (nanohydroxyapatite), alkaline phosphatase (ALP), and nanoclay (MMT). Hydroxyapatite (nHAp) ($Ca_{10}(PO_4)_6(OH)_2$) has a similar mineral composition and structure to that of the human bone tissue and has been used as an implant material since the 1970s.[17,18] nHAp has been well established as a promising biomaterial for bone tissue engineering and regeneration because of its good biocompatibility, strong osteoconductivity, osteoinductivity, and biological activity[19,20] Furthermore, nano-hydroxyapatite (nHAp) with particle size ranging from 1 to 100 nm has the advantage of a

Received: November 8, 2023
Revised: February 23, 2024
Accepted: February 28, 2024
Published: March 25, 2024

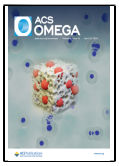

https://doi.org/10.1021/acsomega.3c08877
ACS Omega 2024, 9, 17891−17902

larger surface area to enhance the osteoblast function and to provide intimate contact with surrounding tissues, enhanced biological activity, and low biodegradability.[21,22] The other mineral inducer evaluated in this study is ALP, which is a glycoprotein that acts as an ectoenzyme linked to the outer membrane of cells and matrix vesicles. ALP stimulates extracellular mineralization by releasing inorganic phosphate from the mineralization inhibitor inorganic pyrophosphate.[23,24] Bioceramics have been explored in the field of bone tissue engineering due to their biocompatibility and biodegradability. Recently, silicate bioceramics have attracted a lot of interest as they help in stimulating proliferation, differentiation, osteogenic gene expression of tissue cells, and regeneration of bone tissue mainly attributed to the presence of Si-rich ionic product.[25−27] MMT ($Na^{+}_{0.7}[(Si_8Mg_{5.5}Li_{0.3})O_{20}(OH)_4]^{-}_{0.7}$) used in this study, is a type of synthetic silica clay material, which under physiological conditions can be molded into innocuous, biocompatible biomaterial.[28,29]

The vinyl hydrogels, polyDMAEMA(PD) and polyHPMA-(PH), are prepared by a free-radical mechanism using HEMA as a cross-linker. pHEMA is hydrophilic, gives rise to bioinertness, and enhances cell and protein adhesion properties.[30] The objective of the study was to develop hydrogels from vinyl polymers and understand the type of matrix elasticity that they possess and how that, in turn, dictates cell differentiation of preosteoblasts as well as hBMSCs.

2. MATERIALS AND METHODOLOGY

2.1. Materials. 2-(Dimethylamino)ethyl methacrylate (DMAEMA) (cat. no. 234907), poly hydroxypropylmethacrylamide (pHPMA) (cat. no. 804746), 2-hydroxyethyl methacrylate (HEMA) (cat. no. 477028), ammonium persulfate (APS) (cat. no. A3678), MMT (cat. no. 682659), phosphatase alkaline from bovine intestinal mucosa (ALP) (cat. no. P7640), and lysozyme from chicken egg white (cat. no. L6876) were purchased from SIGMA, and hydroxyapatite (nHAp) (cat. no. 13616) and TEMED (cat. no. 52145) were purchased from SRL.

2.2. Fabrication of Hydrogels. The hydrogels are prepared by a multistep process involving free-radical polymerization and subsequent lyophilization. We have prepared two types of hydrogels: (a) PD and PH hydrogels and (b) PD/PH with nHAp (nHAp)/nanoclay (MMT)/alkaline phosphatase (ALP) mineral inducers. Briefly, PD or PH was added to the tube followed by HEMA and Milli-Q , and then, the chain initiator APS and TEMED were added to the final solution. The solution was vortexed for 10 s and kept at 37 °C for 8 h for complete cross-linking of hydrogels to occur. The purification of the hydrogels after the incubation period was performed by washing the hydrogels with Milli-Q six times. After washing, the hydrogels were kept at −20 °C overnight and then lyophilized for 48 h. For the preparation of nHAp and MMT-based hydrogels, the previous protocol was followed with the addition of 1, 5, and 10 wt % nHAp/MMT in the presence of APS and TEMED. The incubation time, temperature, and washing steps were all kept the same as those of the previous method.

For the preparation of ALP-based hydrogel, the PD/PH hydrogels were prepared, and steps were followed until lyophilization. After complete lyophilization of PD/PH hydrogels, they were treated with 0, 5, and 10 wt % ALP dissolved in 1× PBS solution. Approximately, 120 μL of ALP was used to soak a scaffold cast onto 48-well plates. After 30 min of incubation, beta glycerophosphate calcium hydrate (βGP) was added to the scaffold until the scaffold was immersed completely into it. Every day, the βGP was changed with fresh βGP for 7 days.[23,31] The final hydrogel was washed and freeze-dried by using lyophilization. The reagents used for hydrogel preparation are given in detail in Table 1 (Supporting Information), and the nomenclature of variations used for hydrogel preparation is reported in Table 2.

2.3. Gel Fraction. The scaffolds were analyzed for gel fraction by placing scaffolds inside the 24-well plate, and 1 mL of Milli-Q was poured into each well. The plate was then placed inside the shaking incubator and maintained at 37 °C for 24 h. The weight of the scaffold before being soaked in water was recorded (M_0). After 24 h, the scaffolds were dried with tissue paper using the tap drying method and again freeze-dried before taking the final weight (M) (n = 4). The gel fraction ratio was calculated using the following equation:

$$\text{gel fraction}(\%) = \frac{M}{M_o} \times 100\%$$

2.4. Water Uptake Capacity of the Hydrogels. The scaffolds used for analyzing water uptake were first freeze-dried, and then, the initial weight of each sample was recorded. The scaffolds were then immersed in Milli-Q and maintained at pH 7.4. All of the experiments were continued at room temperature. At regular time intervals, the samples were weighed by removing the excess surface liquid with the help of soft tissue. The percentage of swelling degree (%SD) was calculated to obtain the water uptake of the scaffolds. Here, WS represents the weight of the swollen sample for each time interval and WD represents the initial weight of the scaffolds. The water uptake was performed in quadruplicate, and the %SD was calculated as the mean value:

$$\%\text{SD} = \frac{\text{WS} - \text{WD}}{\text{WD}} \times 100\%$$

2.5. NMR. PD and PH synthesized in the laboratory were characterized by using ^{13}C NMR spectroscopy. ^{13}C NMR analysis was carried out using a Bruker Advance-400.

2.6. TGA-DSC. The thermal behavior of the PD and PH was analyzed using TGA/DSC by using STA 449 F3 Jupiter NETZSCH with a refrigerated cooling system (RCS) facility. Calibration of the system was done by Al_2O_3 standard. The initial weight of the sample was around 15 mg, which was weighed and sealed in aluminum pans. Insulation of the calibration pan was done by maintaining an argon atmosphere. The flow rate of the system was maintained at 80 mL min^{-1} with a 10 °C min^{-1} rise in temperature. Analysis was done until 600 °C both for TGA/DSC.

2.7. Mechanical Properties Using Rheology. The amount of elasticity, complex viscosity, cross-linking, and mechanical strength of the scaffold was analyzed using frequency sweep measurement conducted using a modular compact rheometer (MCR 102E, Anton Paar). The scaffolds were analyzed in parallel plate geometry with a 25 mm diameter. The plates were made of aluminum metal. The force was normalized to 1 N before the test. For the frequency sweep analysis, the frequency was varied from 100 to 0.1 rad s^{-1} at a constant shear strain of 0.1%. All measurements were taken at room temperature. The data points were processed with the inbuilt software Rheoplus, and the storage modulus (G'), complex viscosity (η), loss modulus (G''), etc. were processed from those data points.

https://doi.org/10.1021/acsomega.3c08877
ACS Omega 2024, 9, 17891−17902

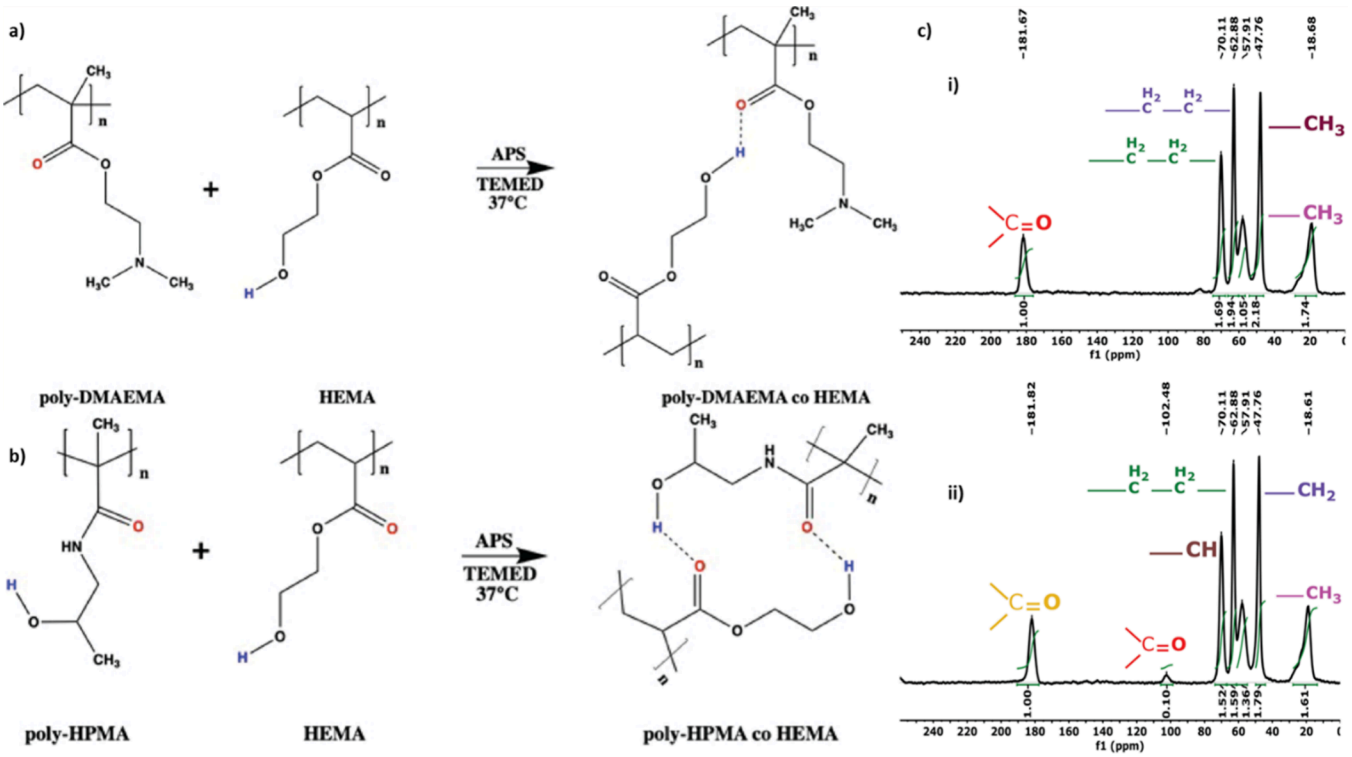

Figure 1. (a) Reaction mechanism of pDMAEMA hydrogel formation. (b) Reaction mechanism of pHPMA hydrogel formation. (c) ^{13}C NMR (400 mHz, Bruker) spectra of (i) pDMAEMA and (ii) pHPMA.

2.8. Surface Morphology. The surface morphology of the scaffolds was investigated using a scanning electron microscopy (SEM) (JEOL JSM-IT800) instrument. The samples were cast into 48-well plates, giving them dimensions of 6−8 mm in height and 8 mm in diameter. Before image processing, the samples were freeze-dried and then coated with a thin gold/palladium (Au−Pd) for 90 s to form a layer by using a plasma magnetron sputter-coater. The porosity of the hydrogel was measured by the software image J by considering $n = 3$ of the images.

2.9. *In Vitro* Cell Culture. The MC3T3-E1 (mouse calvaria preosteoblast, Sigma, cat. no. 99072810-1VL) cell culture was performed in alpha-minimal essential medium (α-MEM, HIMEDIA cat. no. AL221A) with 10% fetal bovine serum (FBS, Gibco Invitrogen, cat. no. 16000044) supplementation, 1% of penicillin-streptomycin (Gibco, Thermo scientific, cat. no. 15140122), and antibiotic solution (0.25%). The amount of antibiotic used was 10 μL of gentamicin (50 mg/mL) for each 50 mL of media prepared for the MC3T3-E1 cell line, and the hBMSCs were cultured in mesencult basal medium with no antibiotics. The hBMSCs cell culture was performed in Mesencult MSC Basal Medium (Human, Stem cell, cat. no. 05401) and was maintained at 37 °C with 5% CO_2. For MC3T3-E1 cell differentiation, media were prepared by adding 500 μL of beta-glycerophosphate (βGP) disodium salt (Sigma, cat. no. G9422) and 100 μL of L-ascorbic acid (Sigma, cat. no. A5960-100G) to complete α-MEM media supplemented with 10% FBS, 0.25% antibiotic solution, and 1% penicillin-streptomycin (Gibco, Thermo scientific, cat. no. 15140122). A stem cell differentiation MesenCult Osteogenic Differentiation Kit (Human, Stemcell, cat. no. 05465) was used for differentiation, and 1.5×10^4 cells on scaffolds were placed in 48-well plates for the alizarin assay and 2×10^3 on scaffolds were prepared in 96-well plates for the PrestoBlue assay.[32]

2.10. PrestoBlue Assay. The cytotoxicity of scaffolds was confirmed using the PrestoBlue assay with the hBMSCs and MC3T3-E1 cell lines. Both cells were grown in 96-well plates (2×10^3 cells per scaffold per well) on hydrogels for 7 days at 37 °C and 5% CO_2. PrestoBlue, a ready-to-use cell-permeable resazurin-based solution, is used to quantitatively measure the viability of the cells by utilizing the reducing power of living cells. On adding the PrestoBlue reagent to the cells, there was a color change from purple to red. This color change can be detected using fluorescence or absorbance measurements. Briefly, 100 μL of PrestoBlue (A 13261, Thermo) reagent was added to every 900 μL of culture media. This reagent was added to each well of 96-well plates containing cell-seeded scaffolds and incubated for 4 h at 37 °C. After 4 h, the fluorescence intensity was measured with a multiplate reader at 535 (excitation)/615 nm (emission).

2.11. Biodegradability of Scaffolds. The biodegradability of scaffolds ($n = 4$) was determined using lysozyme at 800 mg L^{-1} in phosphate-buffered saline solution (PBS, pH = 7.4). The plates were maintained at 37 °C in an orbital shaker at 50 rpm. Enzymatic degradation was monitored for 14 days. Every third day, the lysozyme solution was changed. The samples were removed from the medium after 14 days, rinsed with distilled water, and dried in an oven at 50 °C followed by lyophilization until the mass was constant. The samples were weighed before (m_1) and after *in vitro* degradation (m_2). The degradation degree (Δm) was determined as the weight loss with respect to the initial weight of the sample:

$$\Delta m(\%) = \frac{m_1 - m_2}{m_1} \times 100\%$$

2.12. Alizarin Red Assay. The alizarin red staining method was used to evaluate the amount of calcium deposited on the hydrogel post cell seeding (1.5×10^4) for 7, 14, and 21 days.

https://doi.org/10.1021/acsomega.3c08877
ACS Omega 2024, 9, 17891−17902

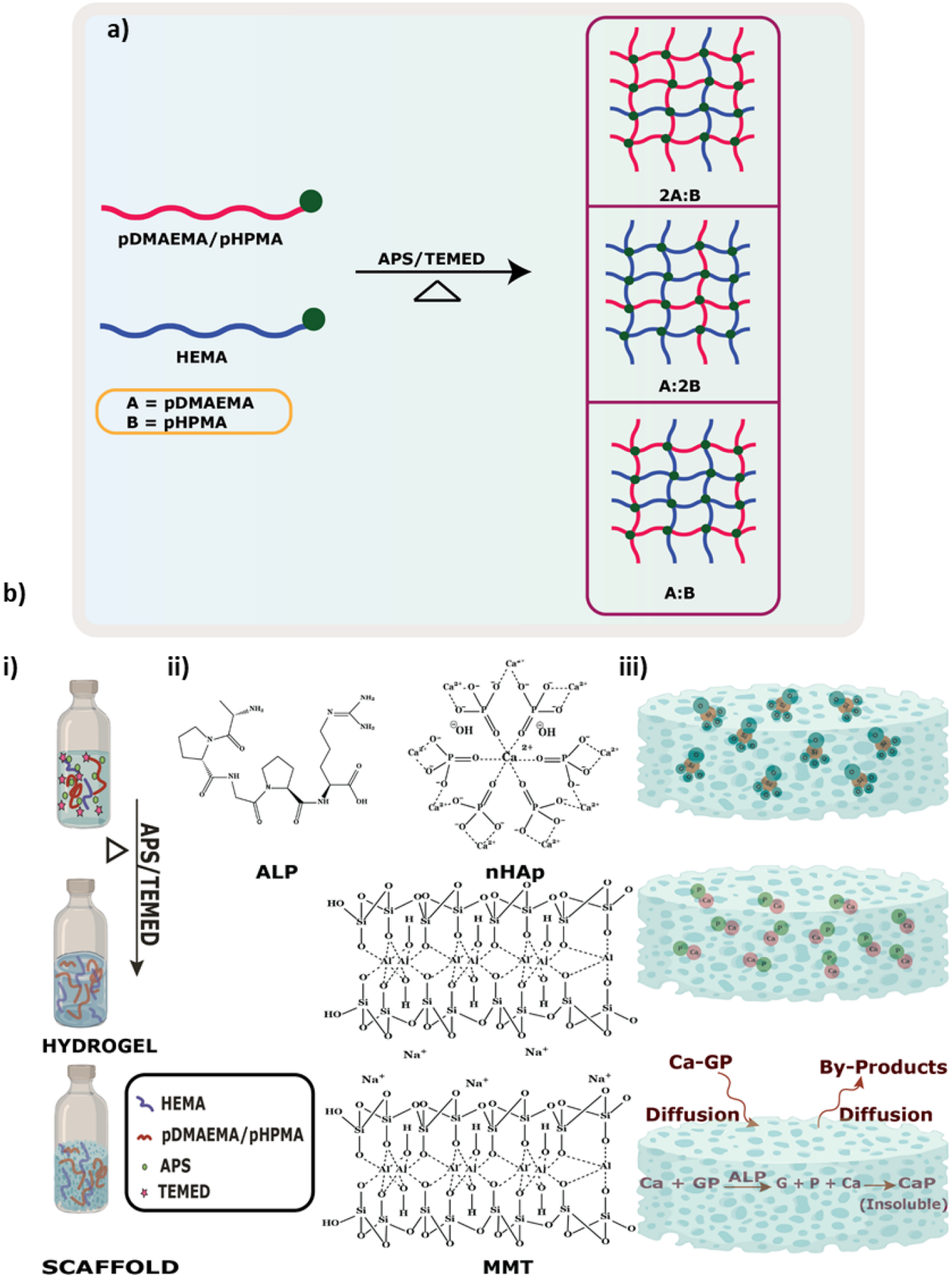

Figure 2. (a) Schematic showing cross-linking while preparation of hydrogel.(b) (i) Schematic showing the formation of PD/PH hydrogels, (ii) structure of mineral inducers used, and (iii) schematic showing the mode of incorporation of mineral inducers. Ca = calcium, GP = beta-glycerophosphate, P = phosphate, CaP = calcium phosphate.

After removal of the medium from each well, the plates were cleaned with a 1× PBS solution. The cells on the hydrogel were then fixed with 4% formaldehyde dissolved in 1× PBS for 20 min at room temperature. After removing the fixation, the scaffolds

https://doi.org/10.1021/acsomega.3c08877
ACS Omega 2024, 9, 17891−17902

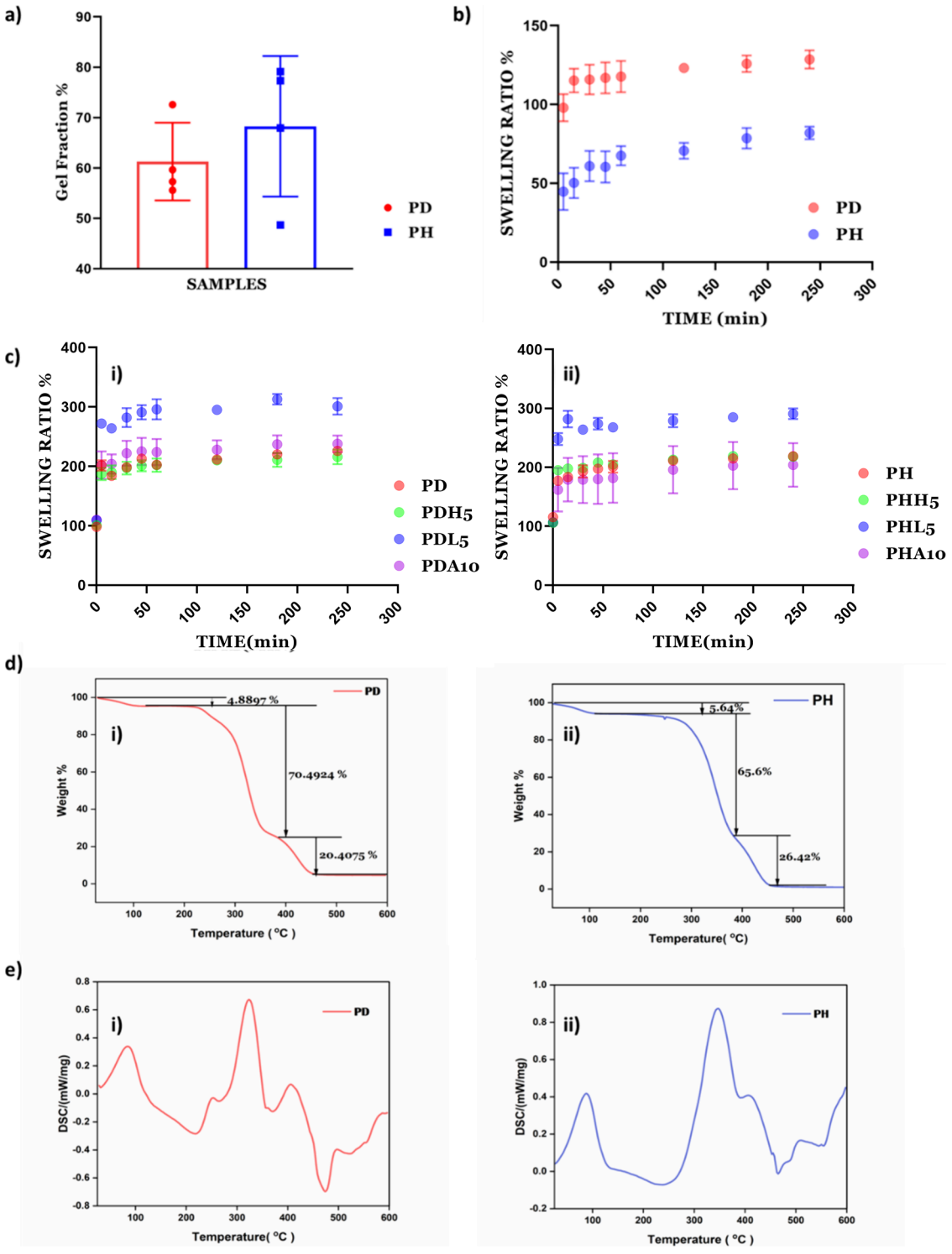

Figure 3. (a) Gel fraction of PD/PH hydrogels, (b) degree of swelling ratio % of PD/PH hydrogels ($n = 4$), (c) (i) swelling ratio % of PD hydrogels ($n = 4$) in all variations and (ii) degree of swelling ratio % of PH hydrogels ($n = 4$) in all variations, (d) TG curves of the (i) PD hydrogel and (ii) PH hydrogel, and (e) DSC curves of the (i) PD hydrogel and (ii) PH hydrogel.

were washed three times with Milli-Q and stained for 20−30 min with 2% alizarin red (Sigma-Aldrich, USA) solution. Then, the scaffolds were washed 3 times with Milli-Q followed by washing with acetone and xylene. The red precipitate was solubilized in 10% cetylpyridinium chloride dissolved in Milli-Q (cat. no. CO732, Sigma-Aldrich, USA), and the optical density was measured at 562 nm to quantify the calcium on the scaffold.

2.13. Statistical Analysis. The quantitative data were expressed as mean ± standard deviation (SD). Statistical analysis was performed using one-way ANOVA in Prism software. Differences between groups of $*p < 0.05$, $**p < 0.01$, $***p < 0.001$, and $****p < 0.00001$ were significant.

https://doi.org/10.1021/acsomega.3c08877
ACS Omega 2024, 9, 17891−17902

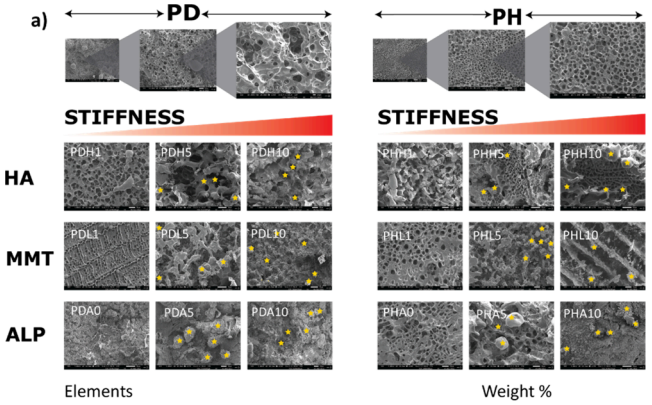

b)

Elements						Weight %		
Samples	C	O	Mg	Al	Si	Fe	P	Ca
PD	54.73	33.33	---	---	---	---	----	---
PDH5	11.20	34.50	---	0.47	0.57	---	13.37	29.23
PDL5	26.23	38.70	2.27	6.17	15.63	---	---	0.83
PDA10	13.97	36.43	---	---	---	2.23	17.00	21.87
PH	51.97	28.73	---	---	---	---	---	---
PHH5	3.00	29.50	---	0.60	0.60	---	17.03	41.27
PHL5	33.07	34.27	1.93	4.20	14.37	---	---	0.90
PHA10	8.43	39.80	---	---	0.67	---	18.20	23.47

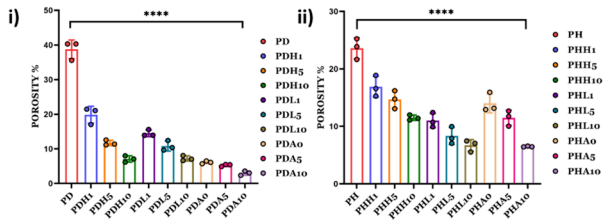

Figure 4. (a) SEM images of PD/PH with all variations of mineral inducers showing the pore nature of the hydrogels. (b) Mineral content of hydrogels calculated by EDAX; (n = 3). (c) Porosity % of (i) PD hydrogels with mineral inducers and (ii) PH hydrogels with mineral inducers, n = 4. (0, 1, 5, and 10 in the nomenclature represent the weight % of mineral inducers added in that particular composition).

3. RESULTS

3.1. Synthesis of pDMAEMA (PD)/pHPMA (PH). PD and PH were formed using a free-radical mechanism with HEMA as the cross-linker. Hydrogen atoms from a hydroxy group of HEMA and the carbonyl group of the pDMAEMA/pHPMA interact through H-bonding, which helps in gel formation (Figure 1a,b). The hydrogels of PD and PH are characterized by ^{13}C NMR spectroscopy (Figure 1). Signals corresponding to the carbonyl groups of DMAEMA are shown at δ = 181.82 ppm (Figure 1c(i)), and ethyl groups of pDMAEMA and HEMA correspond to signals at δ = 57.91, 62.88, and 70.11 ppm and δ = 70.11 ppm, respectively. The methyl group of the dimethylamino group of pDMAEMA has its corresponding signals at δ = 47.76 ppm, and the methyl group of the pDMAEMA group corresponds to δ = 18.68 ppm. Signals corresponding to the carbonyl groups of HPMA and HEMA are shown at δ = 181.67 and 102.48 ppm (Figure 1c(ii)), the ethyl group of pHEMA corresponds to signals at δ = 57.91, 62.88, and 70.11 ppm, respectively. The methyl group of pHPMA has its corresponding signals at δ = 18.61 ppm. The methylene group of pHPMA has its corresponding signals at δ = 47.76 ppm, and the −CH group corresponds to the signal at δ = 70.11 ppm.

3.2. Synthesis of pDMAEMA(PD)/pHPMA(PH)-*co*-poly HEMA Hydrogels and Effect of Mineral Inducers. Two types of hydrogels are prepared using HEMA as a cross-linker, pDMAEMA (PD)- and pHPMA (PH)-based hydrogels. The hydrogels are prepared by free-radical polymerization due to the presence of a carbon−carbon double bond.[33] There are three possible ways of cross-linking taking place where the polymer:-cross-linker ratios can be 2A:B/A:2B/A:B (Figure 2a), leading to hydrogel formation. Preparation of the hydrogel includes the addition of PD/PH, HEMA, and Milli-Q followed by APS and TEMED (Figure 2b(i)). The chemical structures of each mineral inducer are shown in Figure 2b(ii). After successful hydrogel preparation, mineral inducers, namely, nHAp, MMT, and ALP, were introduced to these hydrogels at varied concentrations to obtain hydrogels with varying mechanical strength (Figure 2b(iii)). The vinyl groups present in PD and PH promote the binding of Ca^{2+} ions in an aqueous environment, which provides sites for hydroxyapatite nucleation in the hydrogels, favoring the growth of nHAp crystallites.[34,35] ALP stimulates extracellular mineralization by causing the mineralization inhibitor inorganic pyrophosphate to release an inorganic phosphate. Mineralization begins with the accumulation of calcium and inorganic phosphate, which is then followed by crystal development.[36] The prepared hydrogels contain pores that absorb the ALP solution, which in turn acts on the organic CaP immediately and breaks it down. The enzyme activity is measured at day 0 and day 7, and the ALP activity was seen to gradually decrease after 7 days (Figure S1). The gradual decrease allows the enzyme to breakdown the organic beta-glycerolphosphate and deposit inorganic minerals.

Members of the smectite clay group include montmorillonite, pyrophyllite, saponite, and nontronite. The typical formula for this group's chemical structure is $(Ca,Na,H)(Al,Mg,Fe,Zn)_2(Si,Al)_4O_{10}(OH)_2XH_2O$.[33] Silicate layers with aluminum oxide/hydroxide layer ($Al_2(OH)_4$) in the layer structure are FDA-approved additives in multiple medicinal products and are being used as mineralizing reagents for different hydrogels.[37,38]

3.3. Physicochemical Characterization of the Hydrogels. *3.3.1. Gel Fraction.* The gel fraction considers polymer chains that are covalently linked to the network and is used to calculate the degree of cross-linking. First, the initial weight of the hydrogels is measured, followed by incubation in 2 mL of Milli-Q and incubation at 37 °C for 24 h (as shown in Figure 3a). After 24 h, the final weight is used to calculate the gel fraction. The gel fraction indicates 61.3 and 68% cross-linking for PD and PH, respectively, to form the hydrogels.[39]

3.3.2. Water Absorption Ratio (Swelling Ratio %). The swelling ratio is defined as the fractional increase in the weight of the hydrogels due to water absorption. The swelling ratio is calculated to study water uptake by immersing the scaffolds in Milli-Q at room temperature. The equilibrium swelling is reached at about 4 h and is around 128.64% for PD and 81.94% for PH (Figure 3b). PD showed a higher swelling ratio than the PH hydrogel, which depicts the higher water retention ability of the PD hydrogels compared to PH. The mineral-induced hydrogels show a higher swelling ratio of around 200% compared to only PD (Figure 3c(i)) or PH (Figure 3c(ii)).

3.3.3. Thermal Analysis Using TG-DSC. The thermal stability of the PD and PH hydrogels was investigated using TG analysis. Figure 3d(i) shows the thermal degradation curve of the PD hydrogel sample within a range temperature of room temperature to 600 °C. The decomposition occurs in three steps. The first step occurred in the 100 to 245 °C range, the second is

https://doi.org/10.1021/acsomega.3c08877
ACS Omega 2024, 9, 17891−17902

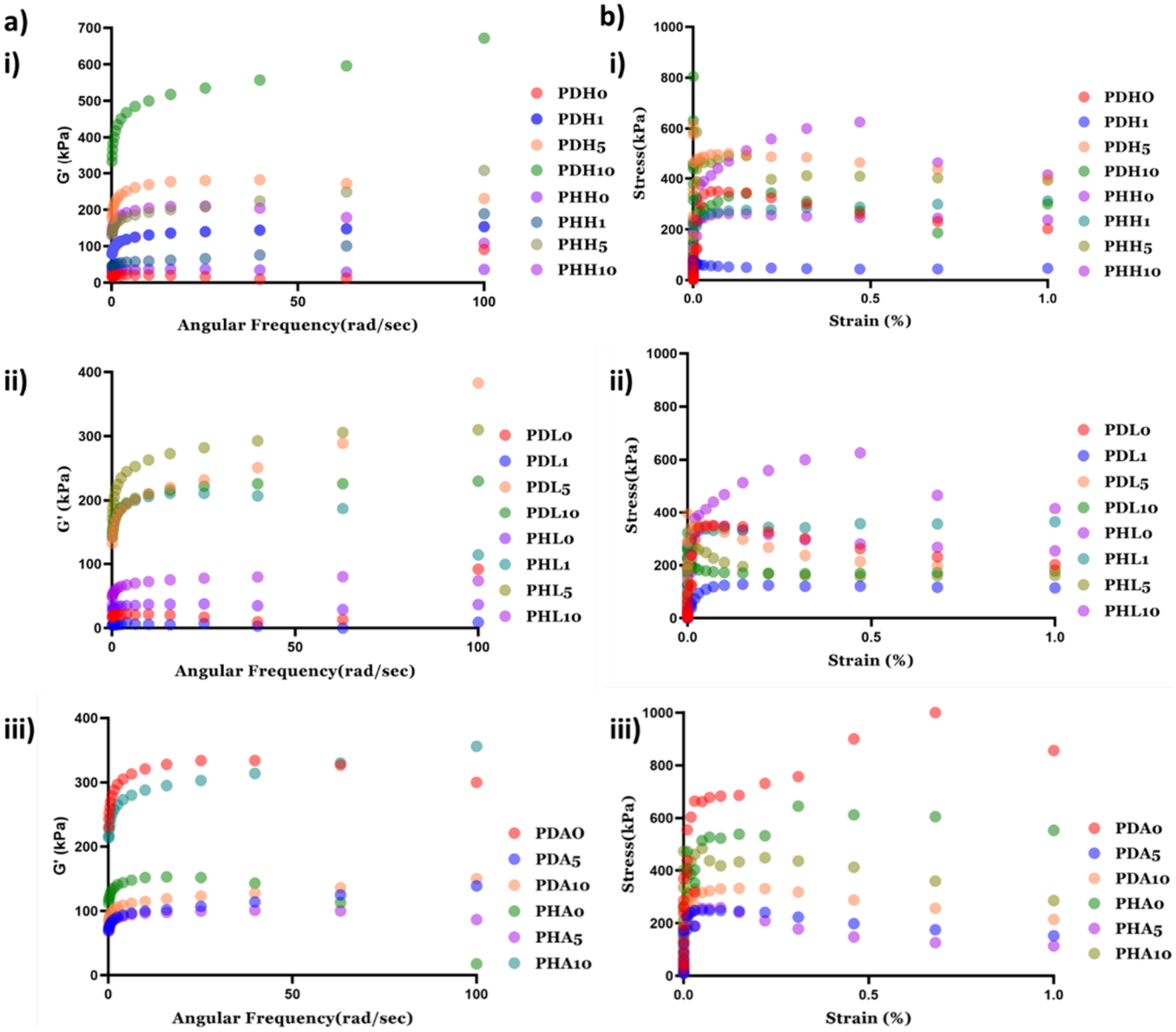

Figure 5. Mechanical properties validated by rheology showing (a) G' vs angular frequency ((i) nHAp-based hydrogels, (ii) MMT-based hydrogels, and (iii) ALP-based hydrogels) and (b) stress vs strain% ((i) nHAp-based hydrogels, (ii) MMT-based hydrogels, and (iii) ALP-based hydrogels). (0, 1, 5, and 10 in the nomenclature represent the weight % of mineral inducers added in that particular composition).

located at 245 to 325 °C, and the third decomposition occurs at 325 to 423 °C, which may be due to the thermal decomposition of side groups and initiation of the disintegration of the main chain.[40] The DSC thermograms of the samples show PD hydrogels (Figure 3e(i)) with an endothermic peak at 90 °C due to water evaporation and at 245 °C showing the first melting of the polymer. The thermogram shows an exothermic peak at 325 and 423 °C related to oxidation and volatile degradation of side groups and initiation of the disintegration of the main chain, respectively.

The thermal stability of the PH hydrogel was investigated using TG analysis. Figure 3d(i) shows the thermal degradation curve of the PH hydrogel samples from room temperature to 600 °C. Here, the decomposition occurs in three steps. The first step occurs in the 100 to 246 °C range, the second is at 246 to 348 °C, and the third decomposition occurs at 348 to 423 °C. The first weight loss corresponds to the loss that occurred due to moisture, the second weight loss occurred at 348 °C due to oxidation and volatile degradation of side groups, and the third weight loss occurred at 423 °C, which may be due to thermal decomposition of side groups and initiation of the disintegration of the main chain.[41] Here, the DSC thermograms of the samples show PH hydrogels depicting an endothermic peak at 90 °C as a result of water evaporation and at 246 °C showing the first melting of the polymer. The thermogram shows an exothermic peak at 348 and 423 °C related to oxidation and volatile degradation of side groups and initiation of the disintegration of the main chain, respectively.

3.4. Morphological Analysis. SEM images of the freeze-dried PD and PH hydrogel with all mineral inducers are presented (Figure 4a). SEM reveals a decreasing porosity with an increase in weight % of mineral inducers and stiffness. The minerals accumulate in pores in the case of nHAp. The increase in concentration of nHAp causes higher mineral deposition in these hydrogels. A higher mineral deposition refers to the Ca:P ratio that is found after forming hydrogels with the

https://doi.org/10.1021/acsomega.3c08877
ACS Omega 2024, 9, 17891−17902

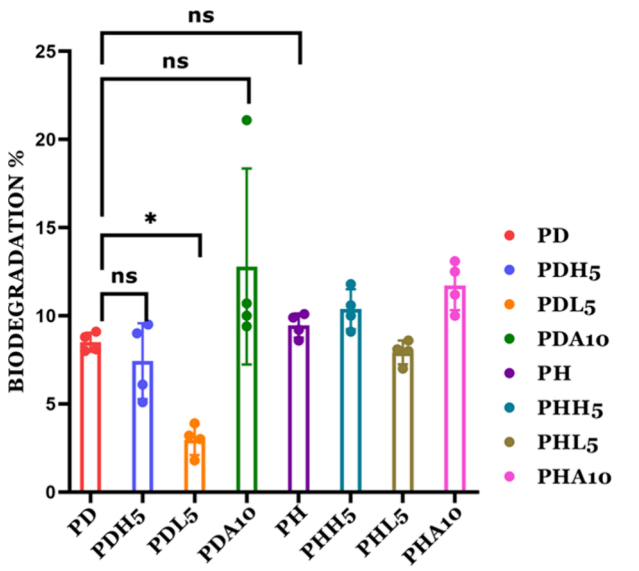

Figure 6. *In vitro* biodegradation of the PD/PH hydrogels when treated with lysozyme enzymes (0, 1, 5, and 10 in the nomenclature represent the weight % of mineral inducers added in that particular composition).

incorporation of mineral inducers. In the case of MMT, increased concentration leads to lesser mineral deposition with varied morphological appearance. Upon treatment with ALP, the deposition of minerals varies between MMT and nHAp (Figure 4b). In the case of nHAp and ALP, Ca and P are predominantly deposited. In the case of MMT, the presence of Si is predominant. Overall, the presence of minerals could be observed in all samples with inducers.

The porosity % (Figure 4c) is calculated to understand the ability of the hydrogel to have a cell−cell interaction. The porosity % values of native PD and PH hydrogels were high as compared to other variations of the mineral inducers, and we could observe that the porosity of the hydrogel decreases with an increase in the % of mineral inducers in comparison to PD and PH hydrogels.

3.5. Hydrogel Mechanical Properties. The storage modulus and loss modulus were analyzed by using rheology. In all the combinations of hydrogels, G' is higher than G''. This data indicates the gel-like behavior of the hydrogel (Figure 5 a). G' and G'' were calculated using angular frequency as a function. From the data, it is seen that the ALP-based hydrogel has a higher G', and the MMT-based hydrogel with 1 wt % MMT showed the least G'. The G' has an increasing trend with an increase in the weight % of mineral inducers used with some exceptions. Figure 5b shows the graph for stress (in kPa) versus strain %. This graph depicts that the stress of the hydrogel increases with an increase in strain %, which means that the strength of hydrogel increases with an increase in percentage of mineral inducers, showing that the mineral inducer-based hydrogels have good mechanical strength for potential bone tissue engineering. From Figure 4 and Figure 5, it was evident that all the types of mineral inducers deposited minerals within the pores of the hydrogels and the mineral-based hydrogels possess good mechanical properties, irrespective of the types of minerals. Eight out of twenty two hydrogels (i.e., PD, PDH5, PDL5, PDA10, PH, PHH5, PHL5, and PHA10) were selected on the basis of mechanical strength aiming support for osteogenic differentiation.

3.6. *In Vitro* Biodegradation. The biodegradation assay is performed on the hydrogels under *in vitro* conditions while mimicking *in vivo* conditions using lysozyme as the enzyme. Approximately, 1.5 μg mL^{-1} to 1 mg mL^{-1} concentration of lysozyme was found to be present in human tissue, depending on the tissue and infection status.[42] The hydrogels did not start degrading until 14 days, offering the possibility of studying the role of matrix stiffness in bone mineralization. Out of the eight selected hydrogels, PDA10 and PHA10 containing ALP showed the highest biodegradability of 12.8 and 11.7%, respectively, while MMT-containing hydrogels showed the least biodegradation %, i.e., 2.97% for PDL5 and 7.92% for PHL5 (Figure 6).

3.7. Effects of Hydrogel Stiffness due to Mineral Inducers on Bone Cells. *3.7.1. Cell Viability and Proliferation.* The viability of the cell on the developed material was validated by a PrestoBlue assay using two types of bone cells, i.e., MC3T3-E1 and hBMSCs. All eight selected variations show positive responses for both cell types, and out of all variations, PDL5 and PHA10 showed the highest cell viability in both cell types. All the hydrogels showed a higher viability than the control, implying that vinyl-based hydrogels can have a wider tissue engineering application (Figure 7a).

3.7.2. Mineralization increases on the overall stiffened matrix of the engineered bone of 3D vinyl hydrogels. The impact of mineralization and bone nodule formation on the increasing stiffness of PD/PH hydrogels is measured using an alizarin assay. Mineralization on days 7, 14, and 21 on these hydrogels is confirmed by using an alizarin red staining assay (Figure 7b). Two types of cell lines, i.e., MC3T3-E1 and hBMSCs, are used. It is observed that ALP-induced hydrogels show a significantly higher mineralization in both the cell type as well as in both the polymer hydrogel (PD/PH). Among the eight selected hydrogels, PDA10 showed a higher mineralization ability compared to PHA10 by 21 days post mineralization. Native hydrogels without cells were taken as a control for the study (Figure S2 and Supporting Information).

4. DISCUSSION

The tissue engineering technique, which uses cells as the building block and provides a scaffold or matrix to guide cell development and matrix formation, is emerging as a subcategory of regenerative medicine. The matrix interaction with the cell has been important in understanding tissue healing and regeneration and has attracted increased attention for reconstructing damaged tissues by using biomimetic strategies. The matrix whose properties predominantly guide the tissue formation has been extensively researched as well. Among many categories of materials that have proven their potential to become suitable matrices, synthetic hydrogels like vinyl polymers allow for tunable biofunctionality as their material properties can be tailored to mimic those of native tissues.[43−46] In this work, vinyl-based hydrogels are considered biomineralized matrices. The matrices are subjected to treatment using different mineral inducers (ALP, nHAp, and MMT), in which matrices with varying mechanical strengths are generated to validate the importance of the matrix in cell proliferation and differentiation. The PD- and PH-based hydrogels have been extensively researched due to their chemical stability, nontoxicity, biocompatibility, biological aging resistance, high water-absorbing capacity, and ease of processing.[47,48]

The hydrogels, PD and PH, have gel fractions of 61.3 and 68%, which quantitatively represents a successful chemical cross-linking (Figure 3a). The water uptake ability of the

https://doi.org/10.1021/acsomega.3c08877
ACS Omega 2024, 9, 17891−17902

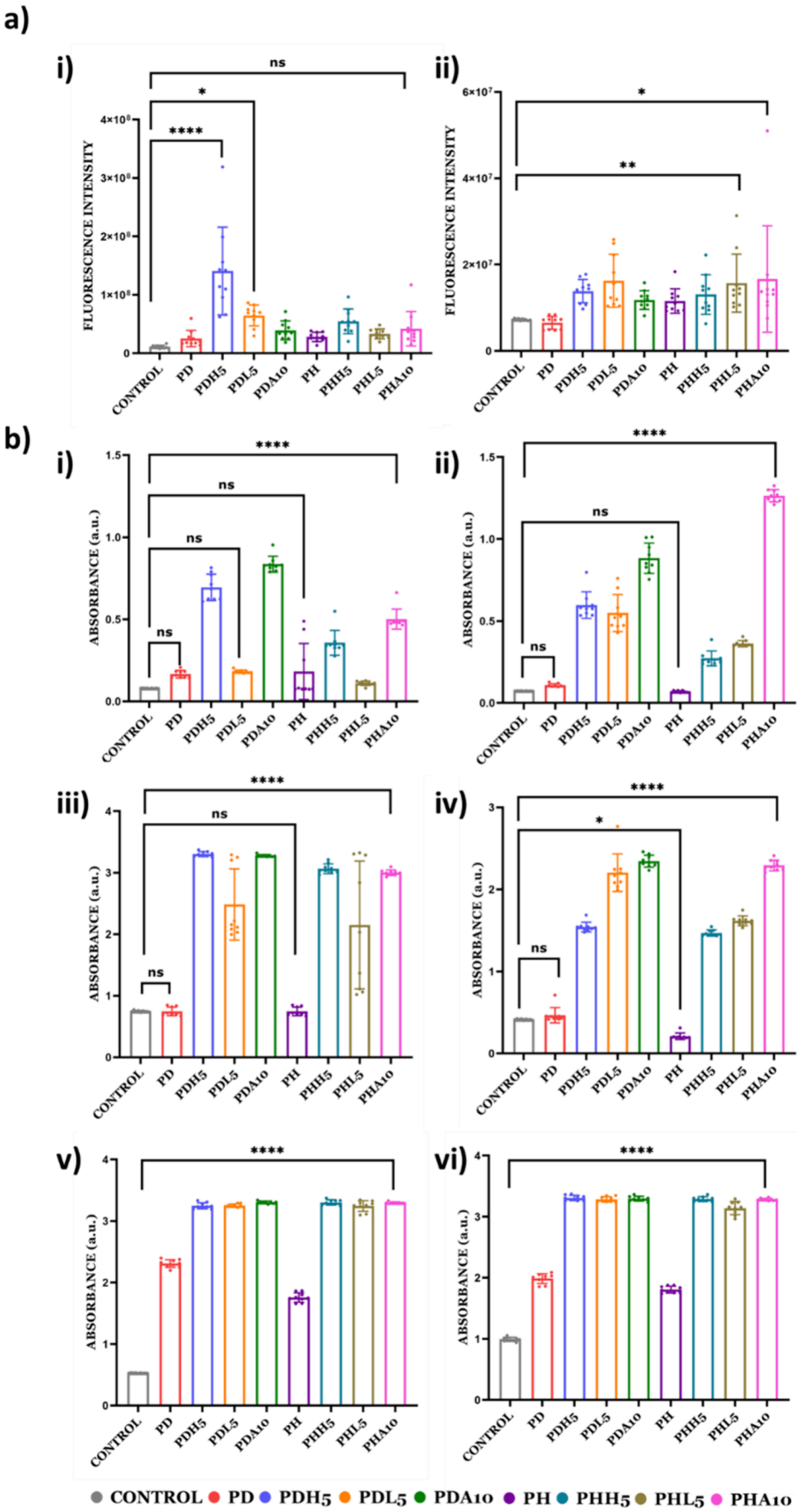

Figure 7. Biological evaluation of hydrogels. (a) Cell proliferation assay by PrestoBlue after 7 days post cell seeding: (i) MC3T3-E1 and (ii) hBMSCs. (b) Mineralization of hydrogels with alizarin red staining of (i) 7 days post cell seeding with MC3T3-E1 on hydrogels, (ii) 7 days post cell seeding with

https://doi.org/10.1021/acsomega.3c08877
ACS Omega 2024, 9, 17891−17902

Figure 7. continued

hBMSCs on hydrogels, (iii) 14 days post cell seeding with MC3T3-E1 on hydrogels, (iv) 14 days post cell seeding with hBMSCs on hydrogels, (v) 21 days post cell seeding with MC3T3-E1 on hydrogels, and (vi) 21 days post cell seeding with hBMSCs on hydrogels. (0, 1, 5, and 10 attached to the nomenclature represent the weight % of mineral inducers added in that particular composition).

hydrogels calculated from the swelling ratio inferred that vinyl-based polymers have the ability to take up cells and allow nucleation sites for mineralization (Figure 3b).

The decreased swelling behavior (Figure 3c(i),(ii)) of mineral-induced hydrogels after a certain duration is due to intense contacts between organic and inorganic phases as well as possible moderate interactions between vinyl groups. These extensive connections produce compact hydrogels with lower media diffusion into the hydrogel network, which alters their swelling behavior.[49] The 3D scaffold breakdown behavior is complex in a dynamic physiological microenvironment and can vary greatly between systems. Weight loss can occur via dissolution or solvation in media, erosion, etching, and enzymatic or hydrolytic cleavage of chains and networks into minute fragments.[50] The thermal stability of the hydrogel, as shown in Figure 3d, shows higher phase change temperatures for the hydrogels. PD and PH variants do not show weight loss up to 100 °C. This means that the fabricated hydrogel is thermally stable for up to 100 °C. Beyond 100 °C, there is a slight change in weight loss, i.e., 4.89% for PD and 5.64% for PH, due to the evaporation of water from the sample up to approximately 245 °C, indicating thermal stability. All the above characterizations indicate vinyl hydrogels to be chemically and thermally stable. In vinyl hydrogels, strong cross-linking in the hydrogel network shields the polymeric chain-breaking site from enzymes.[51] Lower porosity lowers the media penetration and leads to slow disintegration of vinyl-based hydrogels, thus leading to matrices with a slower degradation capability. The hydrogels are subjected to appropriate treatment with three different mineral inducers, namely, ALP, nHAp, and MMT. The three mineral inducers have three different mechanisms of depositing minerals onto the hydrogels.[52] When utilized as implants in the orthopedic, dental, or maxillofacial fields, these mineral inducers have been reported to promote development and osteointegration. In the case of orthopedic implants, the surface of the nHAp mineral-induced implant that is exposed to the surrounding environment binds to natural apatite in the body, promoting bone growth.[53] In ALP- and nHAp-based hydrogels, Ca^{2+} and PO_4^{3-} are secreted from the osteoblasts via vesicles and precipitate in the surroundings. When these hydroxyapatite crystals develop on the polymer matrix, additional mineralization occurs. As a result, the mineralized scaffolds dramatically increase cell activity and callus production for bone repair.[54,55] The MMT-based hydrogel is a synthetic smectite nanoclay that degrades slowly into nontoxic compounds such as Na^+, Li^+, Mg^{2+}, and $Si(OH)_4$, which can promote stem cell proliferation and osteodifferentiation in the absence of exogenous osteoinductive stimuli. MMT nanoplates have a positive charge on their edges and a negative charge on their surface.[28,56] The EDAX report suggests that our mineral-induced hydrogels consist of different forms of minerals required for bone differentiation (Figure 4). Engineered scaffolds with excessive stiffness, for example, impede bone repair due to the stress shielding phenomena.[57] Cells within substrates, on the other hand, sense the stiffness of the surrounding matrix and translate mechanical signals into physiological responses, involving cell proliferation and differentiation. The mechanical strength of the developed hydrogels showed an increased G' rate with an increase in mineral inducer % (Figure 5). The two types of polymer hydrogels (PD/PH) in the presence of different mineral inducers (nHAp, MTT, and ALP) generate a wide variety of hydrogels with different mechanical strengths and stiffness. This also indicates that the PD/PH hydrogel behaves differently from the different mineral inducers. Mechanical strength plays an important role in analyzing the role of hydrogel stiffness in bone context. The mechanical strength increased with increasing cross-linker concentration for both hydrogels because of the resultant stiffer network.[58] The mechanical strength of PD and PH hydrogels with and without mineral inducers is in the range of 5 to 600 kPa. The mechanical strength and mineral content of the bone matrix are around 300 kPa. During the bone healing process, osteogenic progenitor cells adhere and multiply on the implant surface, while calcium and phosphorus are absorbed into the implant surface to precipitate and crystallize for biomineralization, resulting in the production of new bone tissue.[59,60] The hydrogels with different mineral inducers showed different biodegradation profile with ALP based hydrogels having maximum degradability (Figure 6). The proliferation and differentiation of MC3T3-E1 cells and hBMSCs on unmineralized and mineralized substrates are performed to assess whether such alterations may further affect the proliferation and differentiation of cells in the biological environment. The validation of biocompatibility of the hydrogel is done by the PrestoBlue assay, which further proves that the hydrogels are viable for both types of cells (Figure 7a). The presence of mineral-induced matrix stiffness, which in turn had a role in cell mineralization, is validated by the alizarin assay (Figure 7b). These data validated that after 7, 14, and 21 days post cell seeding, the mineral inducer-based hydrogels show enhanced mineralization properties. On day 7, PDH5, PHH5, PDA10, and PH10 show upregulation of mineralization in the MC3T3-E1 cell line, and PDH5, PDL5, PDA10, and PHA10 show upregulation of mineralization in the hBMSC in comparison to the control, indicating the importance of incorporation of mineral inducers in hydrogels. This trend continues for day 21, with similar and comparable observations in both cell lines. However, PDA10 and PHA10 are observed to be efficient from day 7 and can be effectively used as a 3D model for bone tissue engineering.[61,62]

5. CONCLUSIONS

The current study lays down observations on the role of matrix stiffness through mineral inducers in 3D hydrogels to understand alterations in normal bone tissue growth and disease progression during bone loss. Substrate stiffness from mineral inducers has a different influence on cell behavior and fate as per our study. Vinyl-based matrices with different quantities of calcium phosphate mineral inducer can serve as efficient 3D models to study bone mineralization.

https://doi.org/10.1021/acsomega.3c08877
ACS Omega 2024, 9, 17891−17902

■ ASSOCIATED CONTENT

Data Availability Statement

The data is available throughout the manuscript and supporting files.

Supporting Information

The Supporting Information is available free of charge at https://pubs.acs.org/doi/10.1021/acsomega.3c08877.

Material and methodology for ALP activity kinetics of hydrogels fabricated using ALP enzyme; (Table 1) Composition of the reagents used for hydrogel preparation; (Table 2) Nomenclature of all variations of hydrogel; (Figure S1) ALP activity kinetics of hydrogels fabricated using ALP enzyme; (Figure S2) Alizarin assay of native hydrogels without cells (PDF)

■ AUTHOR INFORMATION

Corresponding Author

Mamoni Dash − *Institute of Life Sciences, Bhubaneswar, Odisha 751023, India;* orcid.org/0000-0001-6930-6495; Email: Mamoni.dash@ils.res.in

Authors

Gyanendra Prasad Panda − *Institute of Life Sciences, Bhubaneswar, Odisha 751023, India*

Debyashreeta Barik − *Institute of Life Sciences, Bhubaneswar, Odisha 751023, India; School of Biotechnology, Kalinga Institute of Industrial Technology (KIIT) University, Bhubaneswar, Odisha 751024, India*

Complete contact information is available at: https://pubs.acs.org/10.1021/acsomega.3c08877

Notes

The authors declare no competing financial interest.

#G.P.P. and D.B. have equal contribution. M.D.: conceptualization, validation, formal analysis, investigation, writing (original draft), writing (review and editing), supervising, visualization; G.P.P.: conceptualization, validation, formal analysis, investigation, writing (review & editing), visualization; D.B.: conceptualization, validation, formal analysis, investigation, writing (review & editing), visualization.

■ ACKNOWLEDGMENTS

M.D. acknowledges the Ramalingaswami Fellowship 2016−17 (D.O.NO.BT/HRD/35/02/2006), Department of Biotechnology, Government of India, Department of Biotechnology Grant No. G-17012/1/2020-IFD-DBT, Institute of Life Sciences (ILS), D.B. acknowledges INSPIRE, Department of Science and Technology Government of India, Institute of Life Sciences, DBT-ILS, Sunita Das is acknowledged for her help during SEM. Noemi Scacciati is acknowledged for her valuable input during manuscript preparation.

■ REFERENCES

(1) Stowers, R. S. Advances in Extracellular Matrix-Mimetic Hydrogels to Guide Stem Cell Fate. *Cells Tissues Organs* **2023**, *211* (6), 703−720.

(2) Prouvé, E.; et al. Interplay of matrix stiffness and stress relaxation in directing osteogenic differentiation of mesenchymal stem cells. *Biomaterials Science* **2022**, *10* (17), 4978−4996.

(3) El-Rashidy, A. A.; et al. Effect of Polymeric Matrix Stiffness on Osteogenic Differentiation of Mesenchymal Stem/Progenitor Cells: Concise Review. *Polymers* **2021**, *13* (17), 2950.

(4) Liu, Y.; et al. The stiffness of hydrogel-based bioink impacts mesenchymal stem cells differentiation toward sweat glands in 3D-bioprinted matrix. *Materials Science and Engineering: C* **2021**, *118*, No. 111387.

(5) Varghese, S. A., et al., Chapter 2 - Natural polymers and the hydrogels prepared from them, in *Hydrogels Based on Natural Polymers*, Chen, Y., Ed. 2020, Elsevier. p 17−47.

(6) Sasaki, Y.; Akiyoshi, K. Nanogel engineering for new nanobiomaterials: from chaperoning engineering to biomedical applications. *Chem. Rec.* **2010**, *10* (6), 366−376.

(7) Ida, S. Structural design of vinyl polymer hydrogels utilizing precision radical polymerization. *Polym. J.* **2019**, *51* (9), 803−812.

(8) Sponchioni, M.; et al. Poly(HPMA)-based copolymers with biodegradable side chains able to self assemble into nanoparticles. *RSC Adv.* **2017**, *7* (80), 50981−50992.

(9) Bossion, A.; Zhu, C.; Guerassimoff, L.; Mougin, J.; Nicolas, J.; et al. Vinyl copolymers with faster hydrolytic degradation than aliphatic polyesters and tunable upper critical solution temperatures. *Nat. Commun.* **2022**, *13* (1), 2873.

(10) Ishikawa, S.; et al. Interpenetrating Polymer Network Hydrogels via a One-Pot and in Situ Gelation System Based on Peptide Self-Assembly and Orthogonal Cross-Linking for Tissue Regeneration. *Chem. Mater.* **2020**, *32* (6), 2353−2364.

(11) Douglas, T. E.; et al. Enzymatic mineralization of hydrogels for bone tissue engineering by incorporation of alkaline phosphatase. *Macromol. Biosci* **2012**, *12* (8), 1077−89.

(12) Choudhury, S., et al., Biomimetic Approaches for Biomaterials Development, in *Engineered Biomaterials: Synthesis and Applications*, Malviya, R.; Sundram, S., Eds. 2023, Springer Nature Singapore: Singapore. p 125−152.

(13) Naik, R. R.; Singamaneni, S. Introduction: Bioinspired and Biomimetic Materials. *Chem. Rev.* **2017**, *117* (20), 12581−12583.

(14) Shin, K.; et al. Biomimetic Mineralization of Biomaterials Using Simulated Body Fluids for Bone Tissue Engineering and Regenerative Medicine < sup/>. *Tissue Eng. Part A* **2017**, *23* (19−20), 1169−1180.

(15) Tang, S.; Dong, Z.; Ke, X.; Luo, J.; Li, J.; et al. Advances in biomineralization-inspired materials for hard tissue repair. *Int. J. Oral Sci.* **2021**, *13* (1), 42.

(16) Jin, R.; et al. Biomineralization and osteogenic differentiation modulated by substrate stiffness. *Eur. Polym. J.* **2020**, *122*, No. 109395.

(17) Monroe, E. A.; et al. New Calcium Phosphate Ceramic Material for Bone and Tooth Implants. *Journal of Dental Research* **1971**, *50* (4), 860−861.

(18) Jarcho, M.; Bolen, C. H.; Thomas, M. B.; Bobick, J.; Kay, J. F.; Doremus, R. H.; et al. Hydroxylapatite synthesis and characterization in dense polycrystalline form. *J. Mater. Sci.* **1976**, *11* (11), 2027−2035.

(19) Du, Z.; et al. The effect of carbon nanotubes on osteogenic functions of adipose-derived mesenchymal stem cells in vitro and bone formation in vivo compared with that of nano-hydroxyapatite and the possible mechanism. *Bioactive Materials* **2021**, *6* (2), 333−345.

(20) Zhu, Y.; et al. The Ability and Mechanism of nHAC/CGF in Promoting Osteogenesis and Repairing Mandibular Defects. *Nanomaterials* **2022**, *12*, 212.

(21) Shahrezaie, M.; et al. Effectiveness of tissue engineered three-dimensional bioactive graft on bone healing and regeneration: an in vivo study with significant clinical value. *Journal of Tissue Engineering and Regenerative Medicine* **2018**, *12* (4), 936−960.

(22) Safari, B.; Davaran, S.; Aghanejad, A. Osteogenic potential of the growth factors and bioactive molecules in bone regeneration. *Int. J. Biol. Macromol.* **2021**, *175*, 544−557.

(23) Dash, M.; et al. Ulvan-chitosan polyelectrolyte complexes as matrices for enzyme induced biomimetic mineralization. *Carbohydr. Polym.* **2018**, *182*, 254−264.

(24) Li, N.; et al. Alkaline phosphatase enzyme-induced biomineralization of chitosan scaffolds with enhanced osteogenesis for bone tissue engineering. *Chemical Engineering Journal* **2019**, *371*, 618−630.

(25) Wu, C.; et al. Nagelschmidtite bioceramics with osteostimulation properties: material chemistry activating osteogenic genes and WNT

signalling pathway of human bone marrow stromal cells. *J. Mater. Chem. B* **2013**, *1* (6), 876−885.
(26) Huang, Y.; et al. In vitro and in vivo evaluation of akermanite bioceramics for bone regeneration. *Biomaterials* **2009**, *30* (28), 5041−8.
(27) Loty, C.; et al. Bioactive Glass Stimulates In Vitro Osteoblast Differentiation and Creates a Favorable Template for Bone Tissue Formation. *J. Bone Miner. Res.* **2001**, *16* (2), 231−239.
(28) Atrian, M.; et al. Silk-Laponite fibrous membranes for bone tissue engineering. *Appl. Clay Sci.* **2019**, *174*, 90−99.
(29) Tomás, H.; Alves, C. S.; Rodrigues, J. *Laponite: A key nanoplatform for biomedical applications?* Nanomedicine: Nanotechnology. *Biology and Medicine* **2018**, *14* (7), 2407−2420.
(30) Zhang, L.; et al. Preparation of novel biodegradable pHEMA hydrogel for a tissue engineering scaffold by microwave-assisted polymerization. *Asian Pacific Journal of Tropical Medicine* **2014**, *7* (2), 136−140.
(31) Dash, M.; et al. Enzymatically biomineralized chitosan scaffolds for tissue-engineering applications. *J. Tissue Eng. Regen Med.* **2017**, *11* (5), 1500−1513.
(32) Barik, D.; Bejugam, P. R.; Nayak, C.; Mohanty, K. T.; Singha, A.; Declercq, H. A.; Dash, M.; et al. Polymer-Protein Hybrid Network Involving Mucin: A Mineralized Biomimetic Template for Bone Tissue Engineering. *Macromol. Biosci* **2021**, *21* (6), No. e2000381.
(33) Barik, D.; Kundu, K.; Dash, M. Montmorillonite stabilized chitosan-co-mucin hydrogel for tissue engineering applications. *RSC Adv.* **2021**, *11* (48), 30329−30342.
(34) Han, A.-L.; Rujijanagul, G.; Randorn, C. J. M. L. Preparation of hydroxyapatite hydrogel for bone-like materials via novel self-initiated photocatalytic polymerization. *Mater. Lett.* **2017**, *193*, 142−145.
(35) Ibraheem, S. A.; et al. Novel pectin from Parkia biglobosa pulp mediated green route synthesis of hydroxyapatite nanoparticles. *Surfaces and Interfaces* **2019**, *17*, No. 100360.
(36) Barik, D.; et al. Polymer−Protein Hybrid Network Involving Mucin: A Mineralized Biomimetic Template for Bone Tissue Engineering. *Macromol. Biosci.* **2021**, *21* (6), No. 2000381.
(37) Uddin, F. Clays, Nanoclays, and Montmorillonite Minerals. *Metallurgical and Materials Transactions A* **2008**, *39* (12), 2804−2814.
(38) Wu, M.; et al. Nanoclay mineral-reinforced macroporous nanocomposite scaffolds for in situ bone regeneration: In vitro and in vivo studies. *Materials & Design* **2021**, *205*, No. 109734.
(39) Kampouris, E. M.; Andreopoulos, A. G. Gel content determination in cross-linked polyethylene. *Biomaterials* **1989**, *10* (3), 206−208.
(40) Stawski, D.; Nowak, A. Thermal properties of poly(N,N-dimethylaminoethyl methacrylate). *PLoS One* **2019**, *14* (6), No. e0217441.
(41) Francini, N.; et al. Multifunctional Poly[N-(2-hydroxypropyl)-methacrylamide] Copolymers via Postpolymerization Modification and Sequential Thiol−Ene Chemistry. *Macromolecules* **2015**, *48* (9), 2857−2863.
(42) Reay, S. L.; et al. In vitro evaluation of the biodegradability of chitosan−genipin hydrogels. *Materials Advances* **2022**, *3* (21), 7946−7959.
(43) Ganewatta, M. S.; Wang, Z.; Tang, C. Chemical syntheses of bioinspired and biomimetic polymers toward biobased materials. *Nature Reviews Chemistry* **2021**, *5* (11), 753−772.
(44) Unal, A. Z.; West, J. L. Synthetic ECM: Bioactive Synthetic Hydrogels for 3D Tissue Engineering. *Bioconjug Chem.* **2020**, *31* (10), 2253−2271.
(45) Spicer, C. D. Hydrogel scaffolds for tissue engineering: the importance of polymer choice. *Polym. Chem.* **2020**, *11* (2), 184−219.
(46) Kumar, A.; et al. Polysaccharides, proteins, and synthetic polymers based multimodal hydrogels for various biomedical applications: A review. *Int. J. Biol. Macromol.* **2023**, *247*, No. 125606.
(47) Wang, Y.; et al. Mechanically robust, biocompatible, and durable PHEMA-based hydrogels enabled by the synergic effect of strong intermolecular interaction and suppressed phase separation. *Polymer* **2022**, *254*, No. 125083.
(48) Ho, T. C.; et al. Hydrogels: Properties and Applications in Biomedicine. *Molecules* **2022**, *27* (9), 2902.
(49) Nicolella, P.; Lauxen, D.; Ahmadi, M.; Seiffert, S.; et al. Reversible Hydrogels with Switchable Diffusive Permeability. *Macromol. Chem. Phys.* **2021**, *222* (16), No. 2100076.
(50) Costa, H. S.; et al. Engineered hybrid scaffolds of poly(vinyl alcohol)/bioactive glass for potential bone engineering applications: synthesis, characterization, cytocompatibility, and degradation. *J. Nanomater.* **2012**, *2012*, 4.
(51) Hu, W.; et al. Advances in crosslinking strategies of biomedical hydrogels. *Biomaterials Science* **2019**, *7* (3), 843−855.
(52) Kleber, M.; et al. Dynamic interactions at the mineral−organic matter interface. *Nature Reviews Earth & Environment* **2021**, *2* (6), 402−421.
(53) Anita Lett, J.; et al. Recent advances in natural polymer-based hydroxyapatite scaffolds: Properties and applications. *Eur. Polym. J.* **2021**, *148*, No. 110360.
(54) Li, Z.; et al. Bioinspired mineralized collagen scaffolds for bone tissue engineering. *Bioactive Materials* **2021**, *6* (5), 1491−1511.
(55) Grue, B. H.; Veres, S. P. Effect of increasing mineralization on pre-osteoblast response to native collagen fibril scaffolds for bone tissue repair and regeneration. *J. Appl. Biomater Funct. Mater.* **2022**, *20*, No. 22808000221104000.
(56) Orafa, Z.; Bakhshi, H.; Arab-Ahmadi, S.; Irani, S.; et al. Laponite/amoxicillin-functionalized PLA nanofibrous as osteoinductive and antibacterial scaffolds. *Sci. Rep.* **2022**, *12* (1), 6583.
(57) Yi, B.; Xu, Q.; Liu, W. An overview of substrate stiffness guided cellular response and its applications in tissue regeneration. *Bioactive Materials* **2022**, *15*, 82−102.
(58) Nielsen, L. E. Cross-Linking−Effect on Physical Properties of Polymers. *Journal of Macromolecular Science, Part C* **1969**, *3* (1), 69−103.
(59) Lee, H.-S.; et al. Engineered Phage Matrix Stiffness-Modulating Osteogenic Differentiation. *ACS Appl. Mater. Interfaces* **2018**, *10* (5), 4349−4358.
(60) Salhotra, A.; et al. Mechanisms of bone development and repair. *Nat. Rev. Mol. Cell Biol.* **2020**, *21* (11), 696−711.
(61) Roschger, P.; et al. Changes in the Degree of Mineralization with Osteoporosis and its Treatment. *Current Osteoporosis Reports* **2014**, *12* (3), 338−350.
(62) Bala, Y.; Farlay, D.; Boivin, G. Bone mineralization: from tissue to crystal in normal and pathological contexts. *Osteoporos Int.* **2013**, *24* (8), 2153−66.

https://doi.org/10.1021/acsomega.3c08877
ACS Omega 2024, 9, 17891−17902